THE AMERICAN SOCIETY OF MECHANICAL ENGINEERS
345 E. 47th St., New York, N.Y. 10017

98-GT-326

Investigation of the Circumferential Static Pressure Non-Uniformity Caused by a Centrifugal Compressor Discharge Volute

James M. Sorokes
Cyril J. Borer
Jay M. Koch
Dresser-Rand Turbo-Products Division
Olean, N.Y., USA

ABSTRACT

The paper describes experimental and computational fluid dynamics analyses of the non-uniform static pressure distortion caused by the discharge volute in a high pressure, centrifugal compressor. The experiments described in this paper were done using a heavily instrumented gas re-injection compressor operating at over 6000 psia discharge. Instrumentation was installed to measure static, total, and dynamic pressure as well as impeller strain and mechanical vibrations. A brief description of the compressor and instrumentation are provided.

Concurrent with the experimental work, CFD runs were completed to study the reasons for the pressure non-uniformity. The CFD pressure profile trends agreed well with the experimental results and provided analytical corroboration for the conclusions drawn from the test data.

Conclusions are drawn regarding: a) the response of the non-uniformity to changing flow rates; b) the extent to which the non-uniformity can be detected upstream of the impeller; and c) the mechanical influences of the non-uniformity on the impellers.

INTRODUCTION

Considerable attention has been focused of late on the role that the discharge volute or collector plays in creating unbalanced aero-mechanical forces in a centrifugal compressor. Researchers have found that these components cause distorted pressure fields in the upstream flow passages; i.e., diffusers; and these distortions can lead to adverse effects on the aerodynamic and rotordynamic performance of the compressor. It has long been recognized by manufacturers of pipeline boosters, turbochargers, and other single stage centrifugal products that volutes and other similar components cause unbalanced radial forces that must be addressed when designing rotor bearing systems. Until recently, these forces were not considered significant in multistage centrifugal compressors. However, as demand has grown for higher discharge pressures in gas re-injection compressors, the influence of these unbalanced forces has become of increasing concern. Such forces are believed to cause rotordynamic concerns such as unacceptable levels of subsynchronous radial vibration, and excessive loads on bearings.

This paper presents some findings of a research project undertaken to ascertain the forces contributing to repeated impeller failures on a re-injection compressor installed on an off-shore platform. The general findings of the test program were detailed by Borer et al. (1997). The primary intent of the test program was to measure the aero-mechanical forces acting on the impellers. Special attention was focused on stage three of six as the impeller in the third stage had failed four times despite design changes to both the impeller and its associated stationary hardware. Consequently, sufficient instrumentation was installed to gather data on the various factors which could affect the impeller's operating environment. Of course, two factors distinguished this research program from most prior works. First, the testing was done at ASME PTC-10 Class I conditions; i.e., full load and full pressure with a hydrocarbon gas mixture to virtually duplicate field operating conditions. Discharge pressures in excess of 6000 psia were attained. Second, the stationary hardware in the compressor was heavily instrumented with static pressure taps, total pressure probes, and dynamic pressure transducers. Static and dynamic strain gages were also installed on four of the six impellers. Further discussions of the instrumentation used and its location within the compressor are offered in sections which follow.

Though valuable information was gathered on a variety of aero-mechanical phenomenon; i.e., rotating stall; the focus of this paper will be on the circumferential pressure non-uniformity caused by the discharge volute.

BACKGROUND

Many articles have been published on the pressure fields caused by exit elements. These included the works of Ayder (1993), Fatsis et al. (1995), Moore and Flathers (1996), Jiang et al. (1996), and Flathers

Presented at the International Gas Turbine & Aeroengine Congress & Exhibition
Stockholm, Sweden — June 2–June 5, 1998

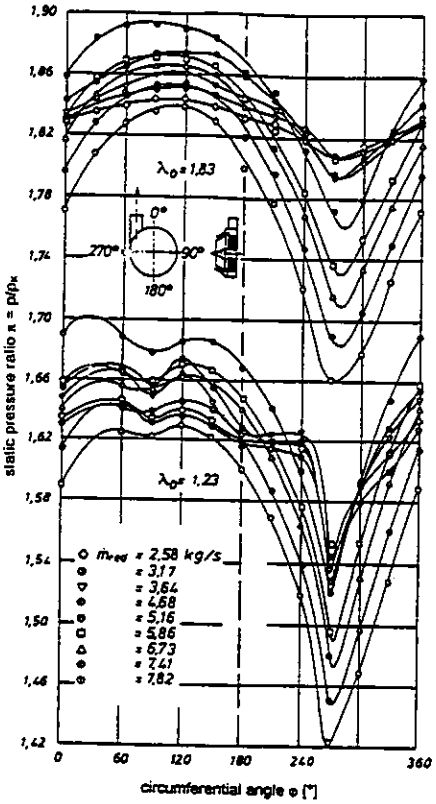

Figure 1. Circumferential static pressure distribution (Hagelstein et al. 1997, Fig. 5)

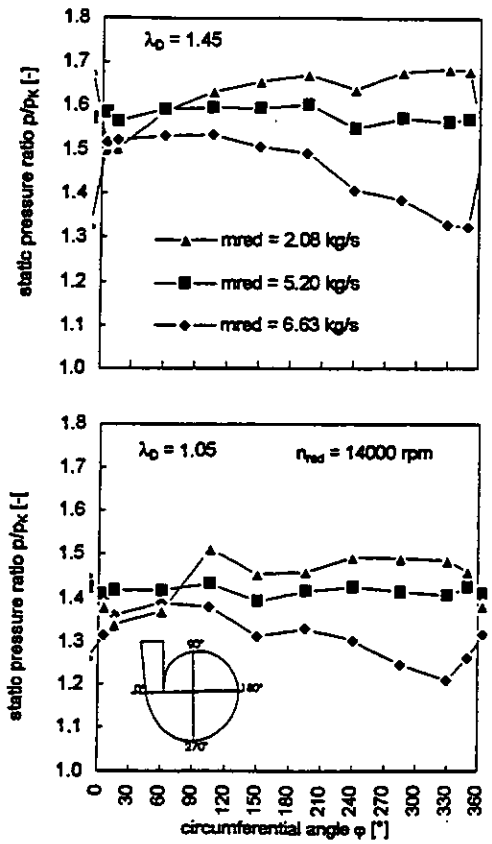

Figure 2. Circumferential static pressure distribution in vaneless diffuser (Hagelstein et al. 1997, Fig. 13)

and Bache (1996). The latter work (Flathers and Bache, 1996) was of particular interest because the authors used computational fluid dynamics to calculate the influence of the volute on the pressure field surrounding an impeller.

More recently, Hagelstein et al. (1997) published a very interesting work detailing the results of their empirical investigation into the circumferential static pressure distortion in centrifugal compressor stages. In their study, they measured the static pressure distribution in several centrifugal configurations. All testing was done with the same test rig which had a maximum pressure ratio of 5:1. The first build tested included a vaneless diffuser and a constant area or concentric collector. The vaneless diffuser was then replaced with various arrangements of vaned diffusers. In the second major build, the concentric collector was replaced by a scroll-type (scheduled area) volute very similar to those used by industrial centrifugal compressor vendors. In both builds, static pressure was measured upstream of the impeller, at numerous radii within the diffuser, and in the collector or volute.

The researcher's measurements clearly showed a non-uniform pressure field within the diffuser. The magnitude of the distortion was quite pronounced in the build with the constant area collector as can be seen in Figure 1. Hagelstein et al. (1997) also noted that the distortion associated with the scheduled area volute was considerably smaller, but only at the stage design flow condition (Figure 2). At off-design conditions, the magnitude of the distortion was nearly equal to that of the concentric collector. They did note some success in using vaned diffusers to attenuate the level of the distortion but even vaned diffusers were not totally successful in eliminating the circumferential variation.

One other observation of Hagelstein et al. (1997) was that while the pressure field at the inlet of the impeller was not constant, the influence of the non-uniform pressure field in the downstream diffuser could not be recognized at the impeller inlet. It is important to note that their research was conducted using an open loop test; i.e., an atmospheric inlet and thus a relatively low inlet pressure.

As noted, this was not the case in the test program described in this paper. The test rig described in this paper operated at inlet pressures of 2600 psia. It is the combination of high inlet pressures and internal instrumentation that distinguishes this testing/analysis from the previous work.

DIFFUSER/VOLUTE CFD ANALYSES

CFD Results -- Diffuser/Volute Analyses

Prior to any of the testing, some basic analytical work had been previously completed to investigate the pressure fields that would occur in a vaneless diffuser followed by a scroll-type discharge volute. The volute for this study was very similar to the volute used in the test rig. The study consisted of several Computational Fluid Dynamics (CFD) runs using the TASCflow code (AEA-ASC, 1997) The model was quite simple; including only the vaneless diffuser and volute and consisted of approximately 120,000 nodes. The inlet conditions into the diffuser (total pressure, total temperature, and flow angle were specified) were assumed constant hub to shroud and uniform

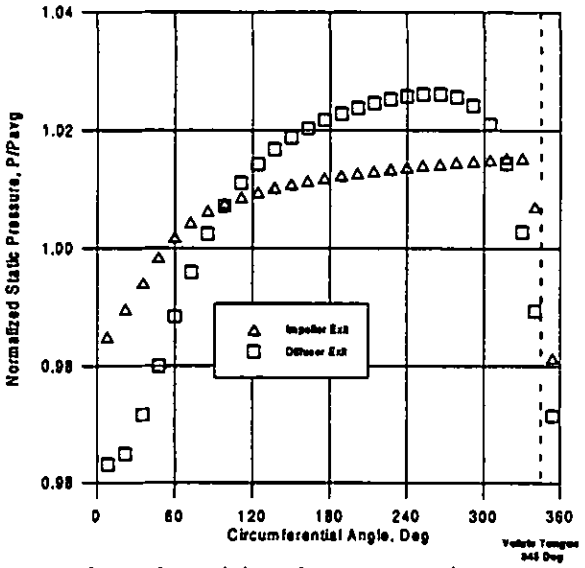

Figure 3. Circumferential static pressure distribution, CFD Results, 70% Design flow (near surge).

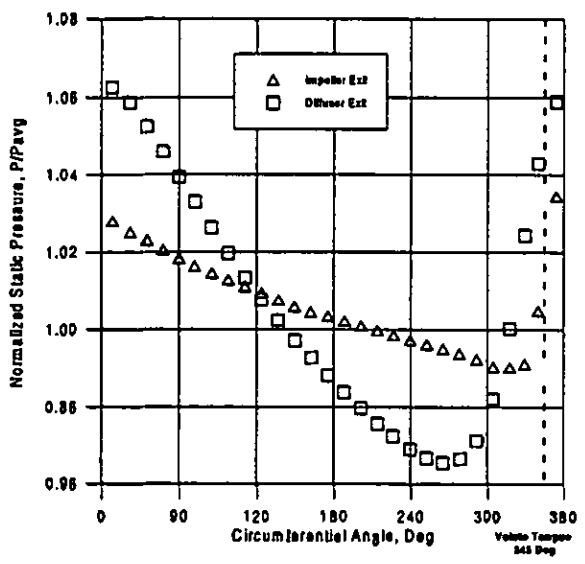

Figure 4. Circumferential static pressure distribution, CFD Results, 150% Design flow (overload).

circumferentially. (At the time the volute study was completed the ability to model both the impeller and volute simultaneously was not available). The resulting hub to shroud velocity distribution was typical of a diffuser following a low to medium flow impeller near design flow; i.e., fairly symmetric about midpassage.

The volute CFD results proved to be extremely interesting because despite the simplicity of the diffuser/volute model, they showed that a non-uniform pressure field was being created around the circumference of the machine. This finding is consistent with those of Flathers and Bache (1996) who analyses clearly showed that flow within the volute and around its "tongue" (or "cutwater") was causing a non-uniform static pressure field and that this field was causing an unbalanced force at the exit of the impeller.

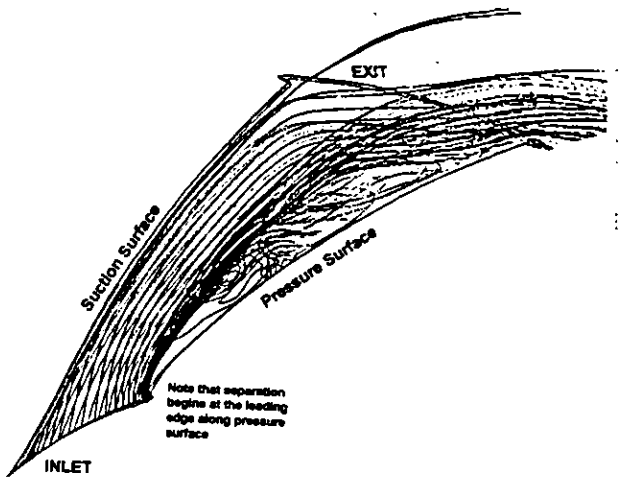

Figure 5. Impeller CFD streakline plots for high flow condition

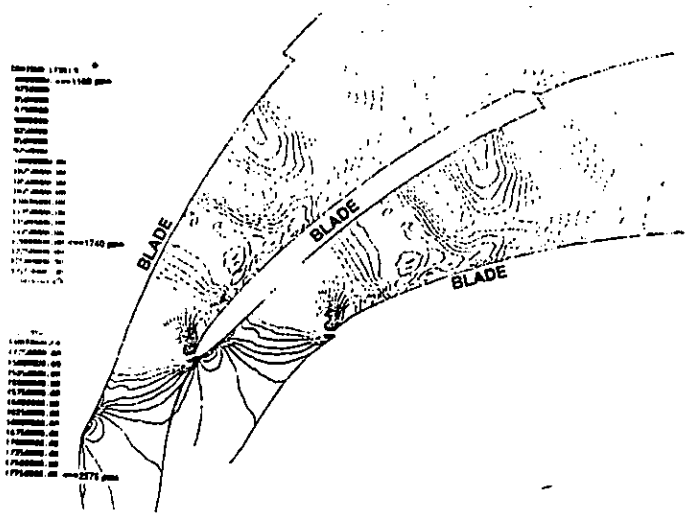

Figure 6. Impeller CFD static pressure contour plot for high flow condition.

The CFD analyses in the current work also indicated that as the flow rate was increased from near surge to overload (or high flow region of the performance map), the magnitude of the pressure variation increased. For illustration, the results provided in Figure 3 are the pressure field in the volute when the stages is running near surge. The "near surge" (70% Design Flow) analyses indicate that the diffuser exit pressure varies by approximately 5% or 400 psia. In Figure 4, the overload (150% Design Flow) condition, the delta P has increased to in excess of 10% or 900 psia. Clearly, the non-uniformity is more severe in overload than at surge.

Also of significant interest, the CFD results suggest that the location of the static pressure minimum moves relative to the volute tongue as the flow is increased from surge to overload. Consequently, the direction of the net force acting upon the impeller will also rotate relative to the volute tongue as the flow rate changes. Note the location of the minimum versus maximum static pressure in the

Table 1:
Compressor Design Point Operating Conditions

	Site	Shop
Inlet Pressure PSIA	**2618**	**2618**
Inlet Temperature, °F	**105**	**105**
Inlet Capacity, ACFM	**744**	**742**
Molecular Weight	**21.85**	**21.85**
Isentropic Exponent	**1.167**	**1.166**
Avg Compressibility Factor	**0.878**	**0.727**
Discharge Pressure, PSIA	**5530**	**5530**
Discharge Temperature, °F	**192.2**	**192.7**
RPM	**10236**	**10299**
BHP	**11081**	**11081**

contour plots given in Figures 3 (near surge) and 4 (overload). The location of the static pressure minima and hence, the direction of the net radial force, has rotated relative to the volute tongue between the two flow conditions.

In addition to a CFD analysis on the volute, another independent analysis was performed on a single passage in the impeller. This work was completed using the BTOB3D code by W. Dawes. This study reviewed many different operating conditions in the impeller. The model consisted of approximately 50,000 nodes and used a velocity specified inlet with a specified downstream pressure. Because this study was completed in support of the impeller failure investigation, the emphasis was on finding any phenomena which may lead to an impeller failure.

Most of the operating conditions reviewed showed nothing extraordinary for this type of low flow impeller. The notable exception was for high flow operating points. At high flows a large leading edge pressure differential results from high negative incidence. The high negative incidence also causes flow separation from the pressure surface, resulting in a very disturbed flowfield within each impeller passage [see Figures 5 and 6]. Due to the high operating pressures, this high pressure differential causes a large mechanical loading in the region of the impeller leading edge.

Having observed these trends in the analytical studies, it remained to be seen if the test data would confirm the existence of the non-uniform pressure field or the level of non-uniformity predicted by the volute CFD analysis.

THE TEST VEHICLE AND INSTRUMENTATION

Conditions

As noted previously, the test program was designed to closely approximate the site operating conditions to permit direct correlation of shop test results to the site (Table 1). The test gas was obtained by on-line mixing of pipeline gas with propane. This gas provided the opportunity to conduct a PTC-10 Class I performance test.

Test Configuration

The compressor tested was a duplicate of the one in the field; although additional drillings, etc. were necessary to accommodate the instrumentation. The unit was installed in a closed loop system on the hydrocarbon test bed at the OEM test facility. The compressor was driven through a speed increasing gear by a steam turbine.

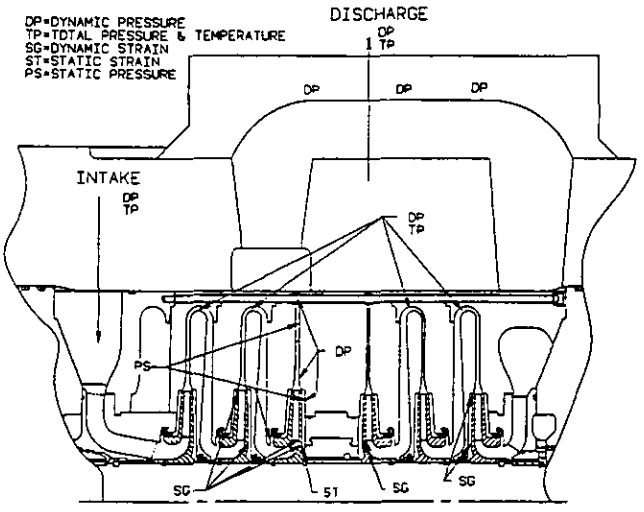

Figure 7. Location of instrumenation in test rig.

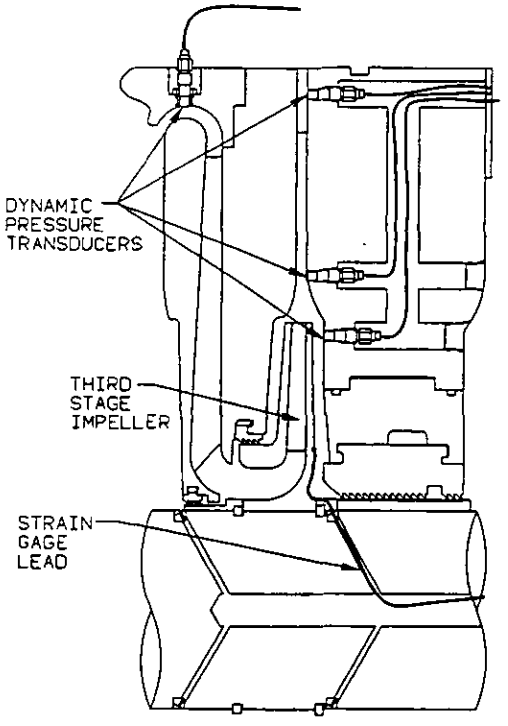

Figure 8. Detail view of dynamic instrumenation for stage 3 of 6 in test rig.

Instrumentation

To meet the test objective, the compressor had to be instrumented to identify the aerodynamic and mechanical forces within the machine. Knowledge of the aerodynamic performance of the compressor was also required to synchronize amplitude and frequency of the dynamic data with location of the compressor on it's operating map.

Instrumentation was concentrated in the area of the third stage since all but one of the failures had occurred in that stage. However, instruments were also installed throughout the machine as conditions leading to the failures may arise upstream (or downstream) of the problem stage (Figure 7).

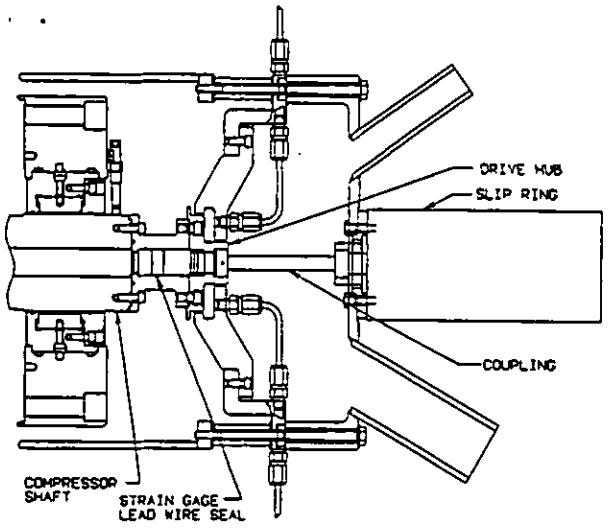

Figure 9. Detail view of slip ring arrangement used to record strain gage measurements.

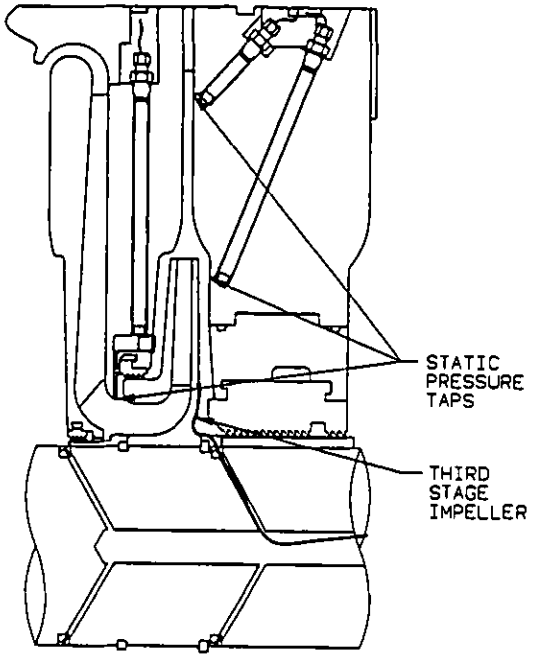

Figure 10. Detail view of steady state instrumenation for stage 3 of 6 in test rig.

To evaluate thermodynamic performance, total temperature and pressure measurements were taken in each stage and at the inlet and discharge of the compressor. Flow was measured using an orifice run located upstream of the compressor inlet. Gas specific gravity was continually monitored and frequent gas samples were acquired to insure known gas properties.

Dynamic pressure probes were employed to detect any transient phenomena that might be contributing to the failures. Dynamic strain gages were applied to impellers to measure the influence of any such phenomena. Static pressure taps were located at the inlet and discharge of the third stage to map the pressure field surrounding that impeller.

Dynamic pressure was measured by high impedance transducers coupled with dual mode charge amplifiers. Nine of these transducers were located internally and five external to the compressor body. A bulkhead connector specially configured for DR use was employed to seal the internal transducer leads at case exit locations. Transducer location and quantity were:

- internal, behind impeller disc, quantity of 2 (Figure 6)
- internal, diffuser wall, quantity of 3 (Figure 6)
- internal, return bend, 1 each for stage 1, 2, 4, and 5 (Figure 6)
- external, crossover channel, quantity of 3
- external, inlet and discharge spool piece, 1 each

Dynamic strain gages were applied to stage 2, 3, 4, and 6 impellers during the different phases of testing (Figure 5). Gages were applied to external (to the primary flow path) disc and cover surfaces and on the impeller blade leading edge as close as possible to the failure site. Lead wires entered the shaft through a tight clearance plug inserted into a radial hole which intersected with a central 3/4 inch bore (Figure 8). A 60 ring mechanical slip-ring coupled to this hub by means of a hollow flexible drive shaft was employed to convert the rotating strain gage signal to a stationary output (Figure 9). Signal conditioning was accomplished by using a specially constructed dynamic stress console consisting of 30 channels of isolated potentiometric strain gage bridge completion.

Shaft displacement was monitored by an industry standard proximity probe and monitor system. Two radial probes were located at each journal bearing and one axial probe was located at the thrust disc.

Signal monitoring was accomplished by use of 14 channels of analog oscilloscope and three channels of FFT spectrum analyzer. All dynamic data was recorded on FM tape recorders. Hydraulic performance data was logged at approximately 20 sec. intervals by a digital data acquisition system.

Static pressure taps were located at 6 points around the circumference at each of (1) the inlet, (2) near the impeller exit, and (3) near the diffuser exit, of the third stage impeller (Figure 10). Steel tubing sealed by a compression gland was used to conduct the static pressures to a bank of 18 pressure transmitters.

Test Operation and Instrumentation Difficulties

The compressor was operated on and outside of its projected flow map (Figure 11). Discharge pressures as high as 6250 psia were achieved during testing at 10,750 rpm. The compressor was intentionally put into stall at four different speeds to investigate stall as a failure cause. The machine was also operated extensively at very high flow rates, including a 20 hour endurance run to assess the effects of operation in deep overload.

Unfortunately, during the testing, several problems were encountered with the instrumentation. Directly affecting the data to be presented in this work, some of the tubes attached to the impeller eye static taps began leaking almost immediately upon reaching the full pressure conditions. Consequently, at no time was a full set of circumferential readings available for the impeller eye pressure distribution. Despite this loss of data, enough information was obtained to draw meaningful conclusions regarding the impeller inlet pressure field.

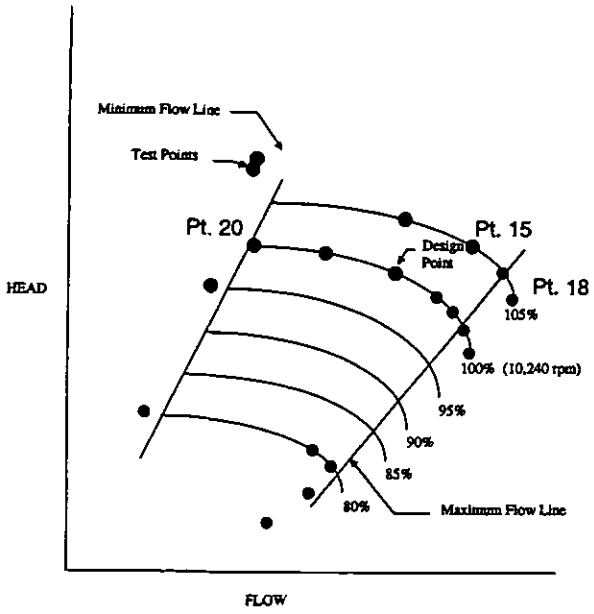

Figure 11. Compressor operating map with test point locations.

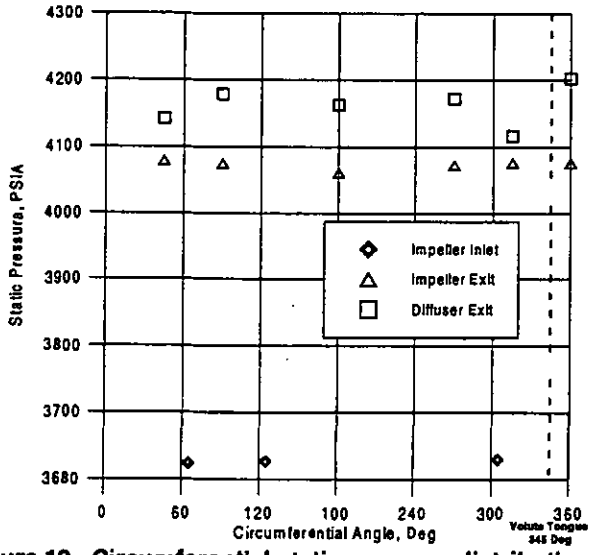

Figure 12. Circumferential static pressure distribution for stage 3 of 6 in test rig, near surge flow, data point 20.

MEASURED DATA

Static Pressure Taps

As noted, static taps were installed at three key locations in the third stage; i.e., the impeller inlet, the impeller exit, and the diffuser exit near the entrance to the volute. Pressure distributions were recorded at several operating conditions across the performance map. However, for conservation of space, only distributions for near minimum stable flow, near design flow, and at maximum flow rates are presented.

The impeller exit and diffuser exit static pressure distributions taken near minimum stable flow (i.e., just prior to onset of rotating stall) are shown in Figure 12. The distributions measured near design

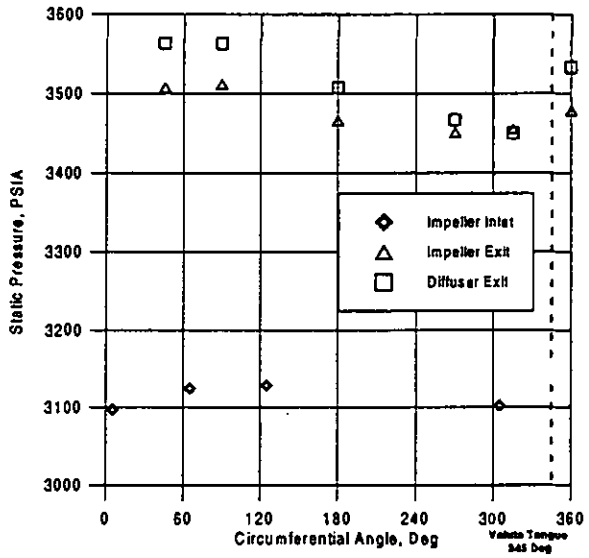

Figure 13. Circumferential static pressure distribution for stage 3 of 6 in test rig, data point 15.

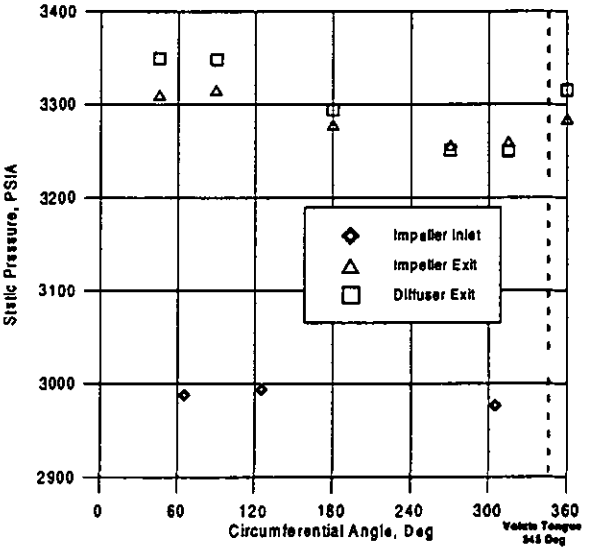

Figure 14. Circumferential static pressure distribution for stage 3 of 6 in test rig, data point 18.

flow are given in Figure 13 while those acquired at maximum flow are illustrated in Figure 14.

Clearly, the distributions are not uniform circumferentially and mimic the trends observed by Hagelstein et al.. Unlike the results of the earlier researchers, there is a substantial difference between the magnitude of the pressure dip at the diffuser and impeller exits. In general, the variation in static pressure at the diffuser exit is approximately twice that at the impeller exit. This trend seems to hold for all three flow conditions.

By comparing the three distributions (Figures 12, 13, and 14), one immediately notes the movement of the minimum static pressure relative to the volute tongue. At minimum stable flow, the minima occurs near the 185 degree position. At design flow, the minima has moved near 300 degrees and at maximum flow, the minima is near 310

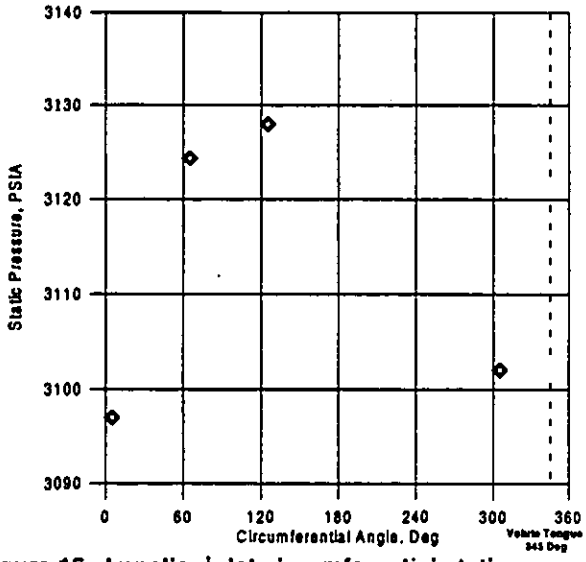

Figure 15. Impeller inlet circumferential static pressure distribution for stage 3 of 6 in test rig, data point 15.

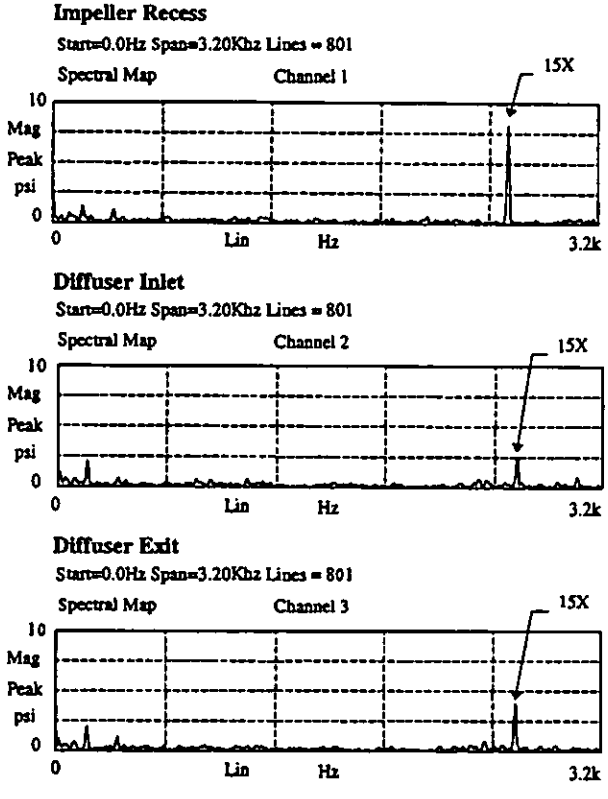

Figure 16. Dynamic pressure response for stage 3 of 6 in test rig, data point 18.

degrees. It is also clear that the magnitude of the non-uniformity is highest at the maximum flow rate.

Of even more importance, the impeller *inlet* pressure distribution showed evidence of the non-uniformity. The static pressure distribution shown in Figure 15 represents the most complete impeller inlet distribution that was acquired prior to the failure of the tubing (noted previously). These taps at the inlet guidevane upstream of the third stage impeller clearly showed a pressure variation around the circumference of the machine. In short, the non-uniform static pressure field is enveloping the impeller. [This should not be too surprising. The compressor inlet conditions will adjust in reaction to the change in downstream pressure. Similarly, the individual flow passages within the impeller will react to a non-uniform downstream pressure. The variation in the individual passages then influences the inlet pressure field upstream of the impeller.]

Dynamic Pressure Probes

The peak amplitude in the pulsations recorded by the dynamic pressure transducers located within the third stage occurred at 15 times running speed (Figure 16). It should come as no surprise that the third stage impeller has 15 blades and that the highest amplitudes were registered at or near the impeller exit. In short, the dynamic pressure probes were sensing the 15 blade wakes.

Reviewing the magnitude of the pressure pulsations, the peak response occurred while the compressor was running in overload. This is not unexpected as the impeller exit absolute velocities would be highest during overload operation, causing the maximum differential between the static pressures in the core and wake regions.

Of interest, the dynamic pressure transducers showed little or no activity near 1X. That is, there was no indication that a one lobe pressure non-uniformity was rotating circumferentially around the compressor. Therefore, it was concluded that the static pressure non-uniformity detected by the static taps was stationary for any given flow condition.

Strain Gages

The strain gages installed on the third stage impeller yielded some interesting trends. The peak response occurred at one times the compressor running speed with little or no noticeable peaks at other frequencies (Figure 17). Like the response in the dynamic pressure transducers and static taps, the amplitude of this 1X excitation was highest when the compressor was running at the overload end of its performance map (Figure 18). A 1X response might be confusing until one recalls that the strain gages are in the rotating frame of reference. Each strain gage will pass through the pressure non-uniformity detected by the static taps once per revolution as the impeller rotates. Since the circumferential static pressure variations both upstream and downstream of the impeller are highest when the compressor is operating in overload, it should follow that the forces acting on the impeller would be maximized at this operating condition.

It was also noteworthy that the circumferential location of the peak dynamic stress detected by the strain gages appeared to move as the flow rate was adjusted from surge to overload. By comparing the phase relationship of the three probes located on the impeller, it was possible to resolve the circumferential location of the maximum response. The rough locations of the peak dynamic strain for the near stall and overload conditions are sketched in Figure 19. These results support the existence of the pressure non-uniformities predicted by the CFD results and measured by the static pressure taps.

Problem Resolution/Status

The testing described in this paper failed to identify the root cause of the impeller failures, but it did provide valuable insight into the forces acting on centrifugal impellers in high pressure applications. A tremendous amount of knowledge was gleaned from this test program

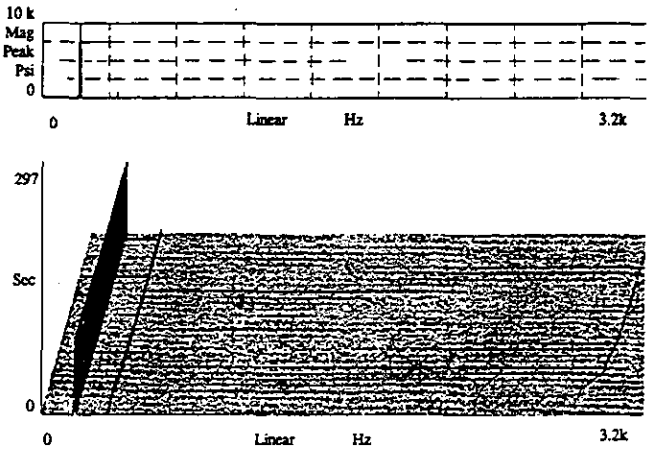

Figure 17. Strain gage measurements for stage 3 of 6 in test rig, data point 18.

regarding the aero-mechanical forces acting upon the impellers in a high pressure, gas re-injection compressor operating at near field conditions. In addition, valuable lessons were learned regarding the use of atypical instrumentation and its associated hardware.

Due to this testing resonance was eliminated as a possible cause. However, testing/analysis did show that overload operation is a prime suspect for the failure because the highest strains were measured in the high flow region of the performance map. Further tests will be conducted that should ultimately lead to the true source of the problems. The information derived from these test programs will be used to develop more reliable and accurate analytical methods in efforts to preclude recurrence of these problems in future machines operating under similar conditions.

Further Considerations

Since it has been established via CFD and test measurements that the pressure is non-uniform at both the impeller inlet and exit, it follows that as the impeller rotates, the individual blades will be subjected to this non-uniform field. In particular, the leading edge of each blade must pass through the non-uniform field once per revolution. The result will be fluctuations in the inlet velocities, Mach numbers, flow angles, pressure profiles, etc. within the various passages. The impeller CFD analyses suggest that a large leading edge pressure differential resulting from high negative incidence caused by overload operation. The high negative incidence also causes flow separation from the pressure surface, resulting in a very disturbed flowfield within each impeller passage [see Figures 5 and 6].

Since each impeller blade passes through the non-uniform field at different times during one revolution, the flow conditions in adjacent passages will vary. In fact, it is highly likely that the conditions within any given blade passage will "fluctuate" due to the non-uniform inlet and exit conditions as the impeller rotates through the skewed pressure field. The non-uniformity in the passage-to-passage distributions will also undoubtedly cause fluctuations in the impeller exit flow profile.

Coupling the observations made in the impeller CFD studies with the fluctuating conditions which likely result in the impeller due to inlet and exit pressure fields caused by the volute, it is not difficult to hypothesize a fairly high dynamic pressure load within the impeller. This dynamic load, if sufficiently severe, could be a major source of

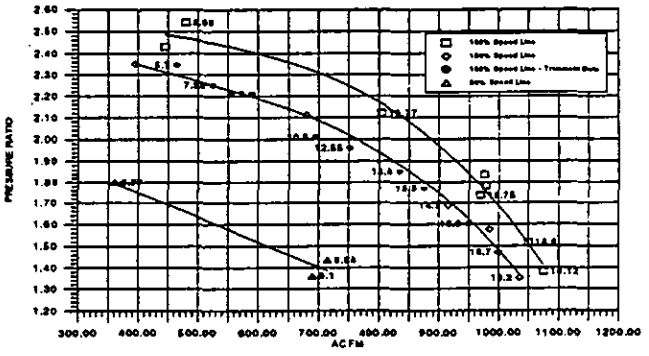

Figure 18. Dynamic Stresses (mean to peak) at impeller leading edge, stage 3 of 6.

the excessive aero-mechanical excitations which caused the impellers to fail. These unsteady flowfields within and around the impeller could also lead to either: a) premature impeller stall or b) a stall in the vaneless space immediately outside the impeller.

Further Analytical Work

There are tremendous complexities involved in trying to understand the aero-mechanical influences of this phenomenon using CFD. The analytical techniques must be capable of accounting for the non-uniform circumferential pressure field and its influence on the impeller inlet conditions. Several CFD codes now have the capability of simultaneously solving the impeller, vaneless diffuser and volute for a steady state solution. The main drawback for this type of problem is grid size and the corresponding solution time. To complete this solution a full 360 degree impeller must be modeled. This necessitates a limit on the impeller nodes to reach a workable problem size of 500,000 to 1 million nodes. Plans are currently in place to complete this steady state analysis.

The previous discussion assumes a stead state solution. But an impeller rotating within a non-uniform pressure distribution will result in transients within the impeller flowfield and an unsteady nature to the impeller's inlet and exit conditions. Since the impeller and diffuser do not operate independently, the fluctuating impeller exit conditions further contributes to the already chaotic nature of the diffuser pressure field. This, in turn, has a "back-influence" on the impeller and creates interaction between the components. Clearly, the transient is an extremely complex problem that is likely beyond the capabilities of most industrial companies and most of today's CFD solvers. It is only with continued research testing, supplemented by steady state CFD analysis, that we will gain further insight into the exact nature of the volute's influence on upstream stage elements.

Further Planned Tests

Plans are underway to perform additional testing using the full load, full pressure test vehicle to investigate methods for eliminating or at least reducing the magnitude of the non-uniform pressure field. In the next phase of tests, the vaneless diffuser following the third impeller will be replaced with a low solidity vaned diffuser (LSD); i.e., similar to the investigation conducted by Hagelstein et al. (1997). The full compliment of instrumentation from the original tests will be left in the compressor and additional probes will be added to help further

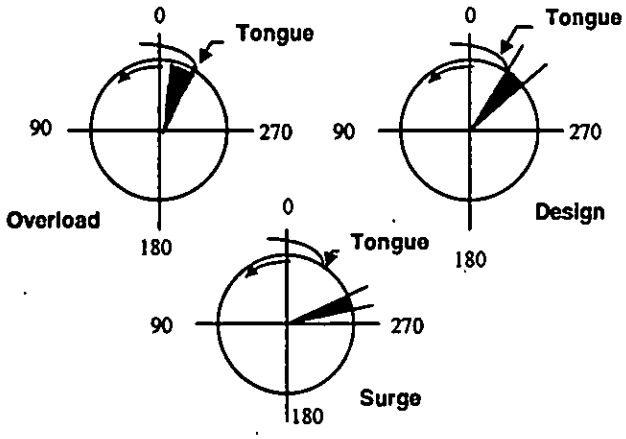

Figure 19. Circumferential location of peak dynamic strain.

resolve the pressure and strain distributions. Additional steps will be taken to extend the life of the static pressure instrumentation to insure that valid results are obtained over the duration of the testing.

Beyond the vaned diffuser testing, some consideration is being given to alternate volute concepts including: alternate area distributions, alternate diffuser styles, "pseudo" or false tongues, etc.

CONCLUSIONS

The results described in this paper represent a portion of data acquired during full load, full pressure testing of a re-injection compressor in an attempt to ascertain the forces contributing to repeated impeller failures. During the testing, sufficient data (static pressures, strain) was obtained to firmly establish the existence of a non-uniform pressure field that enveloped the third stage; which contained an impeller, vaneless diffuser, and discharge volute. The findings of this study are very similar to those obtained by Hagelstein et al. (1997); although their work was conducted using a single stage test vehicle operating at atmospheric inlet pressure.

CFD studies had suggested that a volute would cause a non-uniform pressure distribution in the upstream vaneless diffuser and the test data validated the CFD results. The test data also confirmed that the pressure non-uniformity extends upstream of the impeller; implying that the impeller is subjected to varying inlet and exit conditions. Obviously, if both inlet and exit boundary conditions vary, the passages within the rotating impeller must be highly complex and unsteady. Given the high discharge pressures involved in typical re-injection compressors, it is easy to hypothesize forces sufficiently extreme to contribute to premature stall, rotordynamic difficulties, or even an impeller failure.

The convoluted flowfield involved in the impeller/diffuser/volute arrangement is likely beyond the capabilities of today's CFD solvers. Therefore, research testing remains the most effective means for deriving the information necessary to fully understand the interactions of these flow components.

ACKNOWLEDGMENTS

The authors acknowledge the efforts of Jim Shufelt, Ed Thierman, and Joel Johnson for their assistance in generating the figures used in this paper. The authors also thank: D. Hagelstein and M. Rautenberg of the University of Hannover, Germany for granting us permission to use figures from their paper; Andy Gruss of Measurement Technologies, LTD; and the dedicated members of the Dresser-Rand test department and development lab for their extensive contributions during the test program. Finally, the authors thank Dresser-Rand for allowing publication of this document.

REFERENCES

Ayder, E., "Experimental and Numerical Analysis of the Flow in Centrifugal Compressor and Pump Volutes," PhD Thesis, Von Karman Institute, 1993.

Borer, C., Sorokes, J., McMahon, T., and Abraham, E., "An Assessment of the Forces Acting Upon a Centrifugal Impeller Using Full Load, Full Pressure Hydrocarbon Testing," *Texas A&M Turbomachinery Symposium Proceedings*, 1997.

Fatsis, A., Pierret, S., and Van den Braembussche, R., "3-D Unsteady Flow and Forces in Centrifugal Impellers with Circumferential Distortion of the Outlet Static Pressure," ASME Paper No. 95-GT-33.

Flathers, Michael B., and Bache, George E. "Aerodynamically Induced Radial Forces in a Centrifugal Gas Compressor -- Part 2: Computational Investigation," ASME Paper No. 96-GT-352.

Hagelstein, D., Van den Braembussche, R., Keiper, R., Rautenberg, M., "Experimental Investigation of the Circumferential Pressure Distortion in Centrifugal Compressor Stages," ASME Paper No. 97-GT-50.

Japikse, David, *Centrifugal Compressor Design and Performance*, Concepts ETI Inc., pp 4-12 to 4-21, 1996.

Jiang, Z., Seidel, U., Shao, Z., and Rautenberg, M., "Diffuser, Circumferential Pressure Field and Blade Vibration in a Centrifugal Compressor," 3rd ISAIF, Beijing, China, 1996.

Koch, J.M., Chow, P.N., Hutchinson, B.R., and Elias, S.R., "Experimental and Computational Study of a Radial Compressor Inlet," ASME Paper No. 95-GT-82.

Moore, J. Jeffrey, and Flathers, Michael B., "Aerodynamically Induced Radial Forces in a Centrifugal Gas Compressor -- Part 1: Experimental Measurements," ASME Paper No. 96-GT-120.

Stepanoff, A.J., *Centrifugal and Axial Flow Pumps -- Theory, Design and Application*, 2nd Edition, Wiley Publishing, New York, New York, 1957.

TASCflow Version 2.6 Users Manual, AEA-Advanced Scientific Computing, Waterloo, Ontario, Canada, 1997.